Progress in Composite Materials

Scilight

Article

Effects of Cyclic Cryogenic Treatment on Pure Magnesium and the Effect of Nano ZnO Particles Processed Using Microwave Sintering

Poonam Deshmukh [1], Michael Johanes [2], Dan Sathiaraj [1] and Manoj Gupta [2,*]

[1] Department of Mechanical Engineering, Indian Institute of Technology, Indore 453 552, Madhya Pradesh, India
[2] Department of Mechanical Engineering, National University of Singapore, 9 Engineering Drive 1, Singapore 117 576, Singapore
* Correspondence: mpegm@nus.edu.sg
Received: 30 August 2024; Revised: 27 November 2024; Accepted: 6 December 2024; Published: 9 December 2024

Abstract: The present study, for the first time, reports the effect of cyclic cryogenic treatment (cyclic CT) on pure magnesium and Mg/2 wt.% ZnO (Mg_2ZnO) nanocomposite. Addition of ZnO particles enhanced density of the Mg and nanocomposite material to a maximum of ~30% and ~ 68%, respectively after 2 cycles of CT. Basal plane strengthened after cyclic CT in both materials, irrespective of number of cycles. Addition of ZnO particles showed an enhancement in 0.2 CYS, UCS, fracture strain, and energy absorbed by ~13.88%, ~26%, ~15%, and ~64%, respectively. However, the effect of cyclic CT on pure magnesium was not considerably effective, and properties remained nearly similar to the as-extruded condition. On the contrary, Mg_2ZnO composite material showed a maximum enhancement of ~11%, ~5%, ~8% in 0.2 CYS, UCS, and energy absorbed, while the fracture strain remained constant. Though 1 cycle of cryogenic treatment for pure Mg showed slightly better results, the mechanical properties are almost similar for all cycles. Meanwhile, 2 cycles of cryogenic treatment is more effective in realizing superior combination of mechanical properties in the case of nanocomposite.

Keywords: magnesium alloys; magnesium nanocomposite; cyclic cryogenic composite; compression behavior

1. Introduction

Magnesium is one of the most prominent lightweight structural materials. Magnesium alloys can provide ~33% and ~61% weight savings over aluminum alloys and titanium alloys, respectively [1,2]. Magnesium alloys are light in weight and have exceptional castability, better machinability, and good damping capacity, which makes them suitable candidate materials for structural applications [2]. Therefore, magnesium alloys are widely used for structural applications in the transportation sector (for aerospace, automobile, maritime, and space industries), sports industry, defense sector, and electronics sector due to their capability to mitigate fuel consumption and hence global warming [1–3].

The properties of magnesium alloys degrade considerably after 573 K. Thus, the application is limited to structural components exposed to temperatures ranging from cryogenic to 573 K [4]. However, the limited ductility, elastic modulus, and limited wear and corrosion resistance of magnesium impede its application spectrum [2,5]. This necessitates exploring strengthening methods to enhance the combination of mechanical properties of Mg-based alloys. Reinforcement using metallic or ceramic particles is one of the proven methods to enhance the mechanical properties of magnesium and its alloys. Oxides (Al_2O_3, TiO_2), borides (TiB2, ZrB2), nitrides (BN, AlN), metals (Ti, Mo, Cu) [6–9] etc., are the different types of micron-sized particle reinforcements. Though micro particle reinforcement enhances strength, modulus and wear resistance, it reduces ductility greatly owing to particle cracking and void formation at the matrix-reinforcement interface [10,11]. Further, previous studies have revealed that nano-particle reinforcements have the potential to significantly improve the combination of strength and ductility of magnesium and its alloys [1–3,5,12–16]. For example, investigations on magnesium metal matrix composites using Cu [1], SiC [12], and CeO_2 [13] nanoparticles showed excellent strength with remarkable increase in ductility.

Meanwhile, cryogenic treatment has proven to be a promising post-processing treatment for improving strength and/or elongation and wear resistance [17,18]. Cryogenic treatment (CT) involves exposing materials to

sub-zero temperatures, mostly to liquid nitrogen temperature (−196 °C) [13]. Investigations on cryogenic treatment of Mg-2Nd-4Zn alloy lasting 24, 48, and 144 h resulted in grain refinement, secondary phase precipitation, and change in texture. This led to enhanced plasticity without compromising strength [19]. Experiments on mechanical properties of Mg/2wt.%CeO_2 nanocomposite post-deep cryogenic treatment for 24 h revealed an increase in density, compressive strength and ductility, and microhardness [13]. Further, Gupta et al. [5] performed comparative experimental investigations on microstructure and mechanical properties of Mg/2wt.%CeO_2 after shallow and deep cryogenic treatment. Results indicated that the deep cryogenically treated alloy exhibited superior compressive strength and ductility, ignition resistance, and microhardness.

Accordingly, the present study reports the experimental investigation on compressive mechanical properties of the cyclic cryogenically treated Mg-ZnO nanocomposite. In literature, Tun et al. [3] investigated the effect of ZnO nanoparticle reinforcement on tensile and compressive properties of magnesium nanocomposite. The study suggested that the reinforcement and grain refinement enhanced strength. ZnO nanoparticle reinforcement randomized the basal structure, resulting in increased tensile ductility, but there was no improvement in compressive ductility. Sankaranarayanan et al. [16] added ZnO nanoparticles in different vol.% and reported that the addition 0.8 vol.% of ZnO nanoparticles gave highest mechanical properties. Mg/0.8 vol.% ZnO nanocomposite showed maximum increment of tensile and compressive strength by ~55% and ~95%, respectively. However, effect of cryogenic treatment of Mg-ZnO nanocomposite hasn't yet been explored.

There have been no existing studies in published literature exploring the effect of cyclic cryogenic treatment (cyclic CT) on microstructure and mechanical response of magnesium and magnesium nanocomposites. This study, therefore, focuses to elucidate the synergistic interactive effect of ZnO reinforcement in magnesium nanocomposite and cyclic cryogenic treatment to enhance mechanical properties.

2. Experimental

2.1. Materials and Processing

Magnesium powder (98.5% purity; Merck, München, Germany) of 60–300 µm size is used as a matrix material. ZnO nano-powder (Merck, München, Germany) of 50–200 nm size is used as a reinforcement material. Figure 1 shows the processing steps of Mg-2ZnO composites. Magnesium powder and 2 wt.% ZnO nanopowder were mixed in an Inversina 2L tumbler mixer (Bioengineering AG, Wald, Switzerland) at a speed of 50 rpm for 2 h. The blended powder was then compacted to a 35 mm diameter billet using a hydraulic press. The resulting billets were further processed using microwave-assisted rapid sintering method to 640 °C in a 900 W microwave oven. SiC powder was used as the susceptor material due to its inherent desirable characteristics [1]. A 150-ton hydraulic press was used to hot extrude magnesium and magnesium nanocomposite billets at a extrusion ratio of 20.25:1 and a rod with diameter of 8 mm was synthesized. The extrusion was conducted at 350 °C after prior homogenization at 400 °C for 1 h. Figure 2 shows the elemental mapping results confirming uniform distribution of the elements. Besides, ZnO particles are saturated in the vicinity to cracks.

As-extruded (AE) rods were then sectioned into samples of 8 mm diameter and 50 mm length for further characterization. Both materials were subjected to three different cycles of cryogenic treatment at liquid nitrogen temperature. The cyclic CT consists of 1, 2, and 3 alternate cycles of cryogenic treatment and holding at room temperature for 24 h each, as elaborated in Figure 3. Thus, the material under investigation is labelled according to the processing condition as depicted in Table 1.

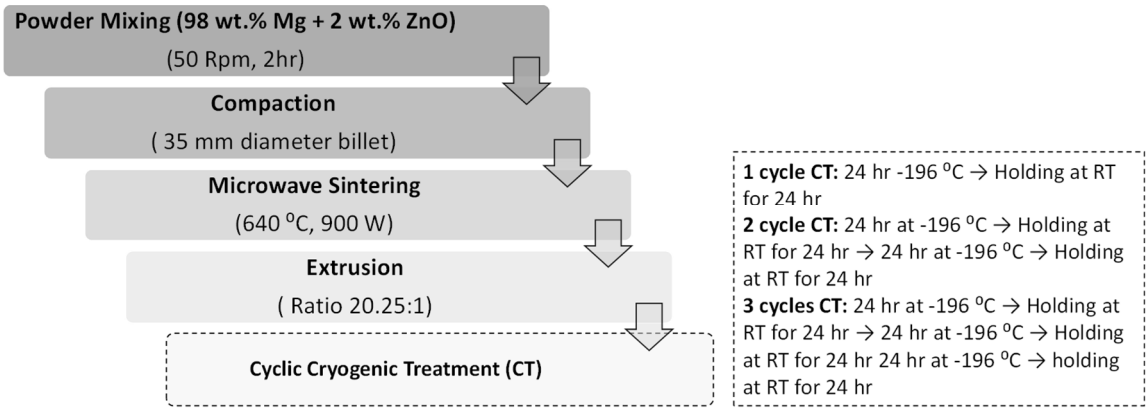

Figure 1. Flowchart presenting processing of Mg2ZnO composites.

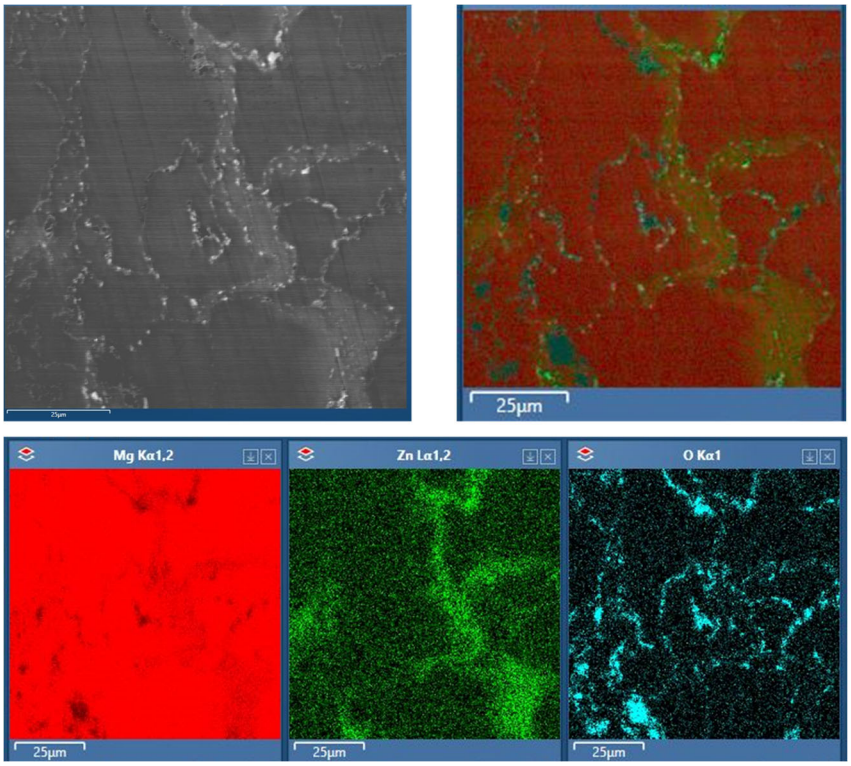

Figure 2. EDS Elemental mapping of as-extruded Mg2ZnO nanocomposite**.**

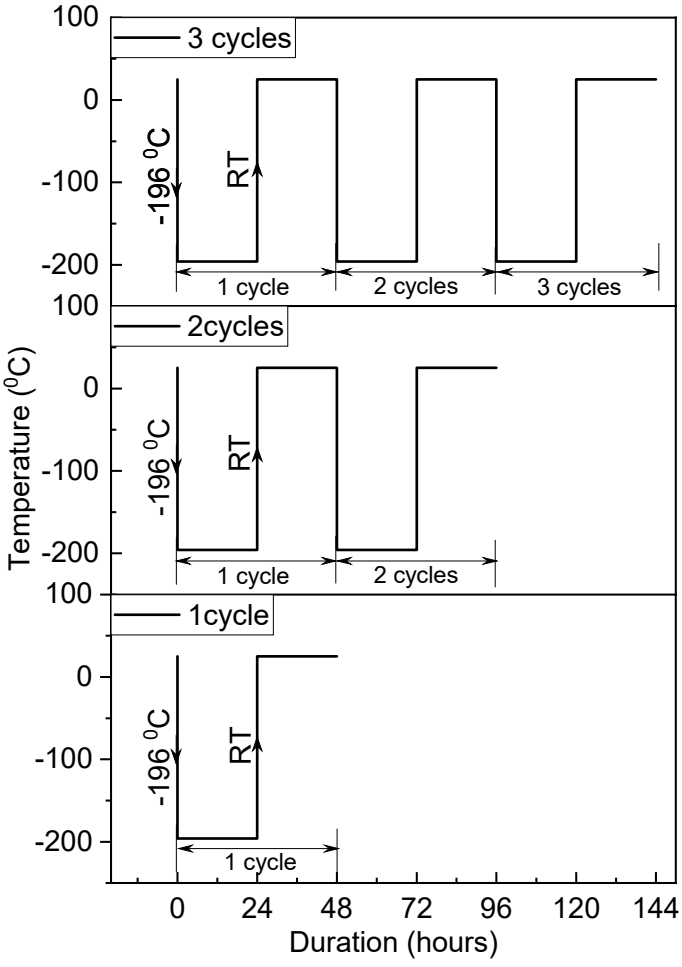

Figure 3. Temperature cycles of materials subjected to cyclic cryogenic treatment.

Table 1. Material labelling according to processing condition.

Material/Processing Condition	Label
As-Extruded Mg	Mg AE
Mg 1 cyclic CT	Mg–1 cycle
Mg 2 cyclic CT	Mg–2 cycles
Mg 3 cyclic CT	Mg–3 cycles
As-Extruded Mg/2 wt.% ZnO nanocomposite	Mg2ZnO AE
Mg/2 wt.% ZnO nanocomposite 1 cyclic CT	Mg2ZnO–1 cycle
Mg/2 wt.% ZnO nanocomposite 2 cyclic CT	Mg2ZnO–2 cycles
Mg/2 wt.% ZnO nanocomposite 3 cyclic CT	Mg2ZnO–3 cycles

2.2. Characterisation

The Archimedes principle was used to measure experimental density before and after cyclic cryogenic treatment (cyclic CT) with the AND GH-252 electronic balance equipped with the AD-1653 Density Determination Kit (AND Company, Limited, Tokyo, Japan). Four samples per condition were used for density measurements. The rule of mixtures was utilized to evaluate the theoretical density of Mg/2wt.%ZnO nanocomposite.

For metallographic sample preparation, samples were first ground successively using 1000 and 4000 grit size emery papers. Further, the silica suspensions of 1, 0.5, and 0.05 μm were used to polish the samples. DI water was used during grinding and polishing to avoid oxidation. In the last step, samples are washed in DI water and dried immediately to prevent oxidation.

Microstructural characterization was conducted using a Leica DM2500 optical microscope (Leica Camera AG, Wetzlar, Germany) to evaluate average grain size and distribution. The chemical etchant used was 5% citric acid in de-ionized water. ASTM E112-13 (2021) was followed for the grain size evaluation. Grain size measurements were performed using MATLAB (version 2013b, MathWorks, Carlsbad, CA, U.S.).

The elemental mapping was performed using HITACHI S-4300 field emission scanning electron microscope (FESEM, Hitachi Ltd., Tokyo, Japan) equipped with an EDS attachment (Hitachi Ltd., Tokyo, Japan).

X-ray diffraction studies were conducted to observe strengths of different peaks using the Shimadzu Lab-XRD 6000 automated spectrometer (Shimadzu Corporation, Kyoto, Japan). Samples prior to and after cyclic cryogenic treatment were scanned using CuKα radiation of 0.154056 nm along the longitudinal direction at a scan speed of 2 °C min^{-1}.

Damping test was conducted as per ASTM E1876-09 standard to determine elastic modulus and damping behavior using the RFDA software (version 8.1.2., IMCE, Belgium). Damping test samples were of 7 mm diameter and 50 mm length.

Hardness measurements are carried out using a Shimadzu-HMV automatic digital microhardness tester equipped with a Vickers indenter, and ASTM standard E384-08 is followed for the test. Vickers hardness test is performed at a load and dwell time of 245.2 mN and 15 s, respectively.

Room temperature compression test was performed as per ASTM E9-09. A MTS-E44 servo-hydraulic tester (MTS Systems, Eden Prairie, MN, USA) was used to measure compressive properties at a strain rate of 5×10^{-3} min^{-1}. Three samples per condition with a diameter to length ratio of 1 were tested. The fractured surfaces were analysed using HITACHI S-4300 FESEM (Hitachi, Ltd., Tokyo, Japan) to observe the mechanisms and modes of fracture.

3. Results and Discussion

3.1. Density and Porosity

Figure 4 presents SEM micrographs showing porosity in Mg and Mg2Zno before and after cyclic CT. The density and porosity values (with standard deviation) of Mg and Mg/2 wt.% ZnO nanocomposite (Mg2ZnO) are as depicted in Table 2. The experimental density ($\rho_{experimental}$) of Mg samples was observed to be increased after 1 cycle and 2 cycles CT while the Mg–3 cycles showed maximum reduction in porosity of ~69%. The porosity reduction of ~30% was achieved for Mg–1 cycle and Mg–2 cycles samples after cyclic CT. Mg2ZnO nanocomposite showed considerable increase in density after all cycles of CT. However, the maximum $\rho_{experimental}$ was obtained for Mg2ZnO–2 cycles sample with ~68% reduction in porosity. The decrease in porosity after cyclic CT indicated the capability of cryogenic treatment to obtain denser Mg2ZnO nanocomposites. The reduction in porosity could be attributed to the induced compressive stresses which causes inward deformation of pores, and

ability of pores to act as a reservoir for dislocations which are typically formed during CT [20–22]. In the current work, porosity is reduced after all cyclic CTs. The reduction in porosity with increased number of cycles of CT could be attributed to the higher compressive stresses. However, average porosity in Mg2ZnO–2 cycles is similar to Mg2ZnO–3 cycles sample considering the standard deviation.

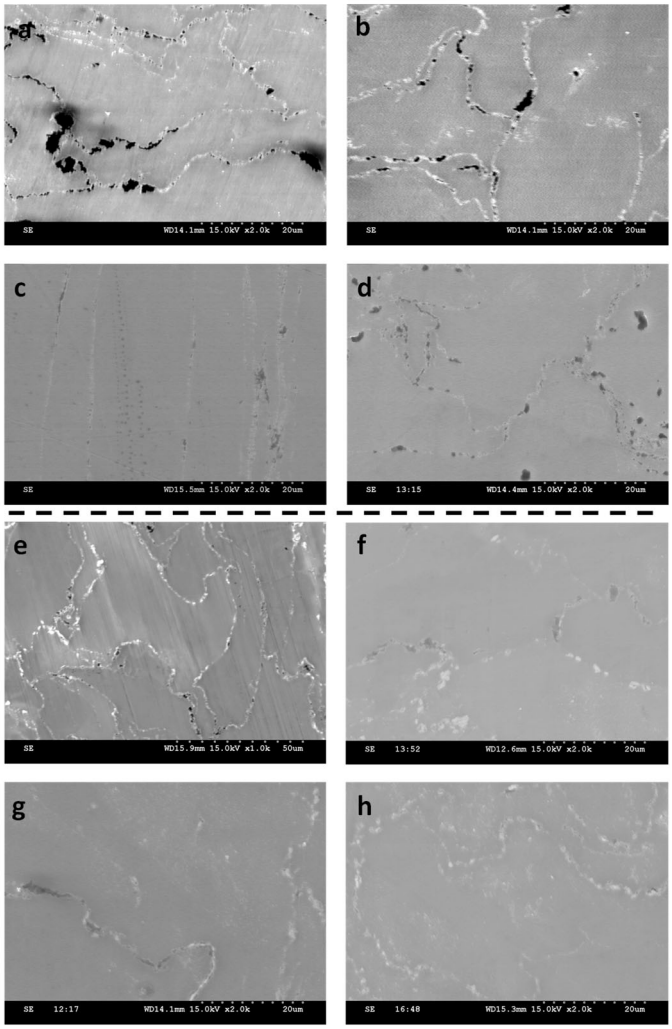

Figure 4. SEM micrographs showing porosity in different samples (**a**) Mg AE, (**b**) Mg–1 cycle, (**c**) Mg–2 cycles, (**d**) Mg–3 cycles, (**e**) Mg2ZnO AE, (**f**) Mg2ZnO–1cycle, (**g**) Mg2ZnO–2 cycles, (**h**) Mg2ZnO–3 cycles.

Table 2. Density and porosity measurements before and after cyclic CT.

Material	Theoretical Density ($g.cm^{-3}$)	Before		After		Change in Porosity (%)
		$\rho_{experimental}$ ($g.cm^{-3}$)	Porosity (%)	$\rho_{experimental}$ ($g.cm^{-3}$)	Porosity (%)	
Mg–1cycle	1.7380	1.7318 ± 0.003	0.356 ± 0.063	1.7337 ± 0.0077	0.248 ± 0.049	30 (↓)
Mg–2 cycles	1.7380	1.7352 ± 0.002	0.163 ± 0.035	1.7360 ± 0.0015	0.114 ± 0.087	30 (↓)
Mg–3 cycles	1.7380	1.7314 ± 0.002	0.379 ± 0.058	1.7360 ± 0.0004	0.115 ± 0.023	69 (↓)
Mg2ZnO–1 cycle	1.7623	1.7561 ± 0.002	0.355 ± 0.105	1.7567 ± 0.0008	0.321 ± 0.046	10 (↓)
Mg2ZnO–2 cycles	1.7623	1.7560 ± 0.003	0.357 ± 0.046	1.7603 ± 0.0007	0.115 ± 0.037	68 (↓)
Mg2ZnO–3 cycles	1.7623	1.7558 ± 0.002	0.369 ± 0.110	1.7576 ± 0.0024	0.266 ± 0.035	28 (↓)

3.2. Microstructure Studies

As shown in Figure 5, microstructure studies are performed to obtain the average grain size before and after cyclic CT of Mg and Mg2ZnO nanocomposite. There was no or negligible grain refinement in the composite in AE condition after addition of ZnO nanoparticles. Although there was a reduction in average grain size of both materials after every cyclic CT when compared to AE samples, the grain refinement was not significant and values fell inside the standard deviation. However, Mg–2 cycles sample showed noticeable average grain size refinement of ~23% from 26 to 20 μm. Figure 6 shows grain size distribution for both materials in AE condition and after

cyclic CT. Mg AE and Mg–1 cycle samples showed bimodal grain size distribution, indicating a combination of fine and coarse grains. Mg–2 cycles samples showed grain size distribution skewed on the left side, indicating many fine grains and very few coarse grains. Grain size distribution was more homogenous, but the spread of the curve more towards the left indicated a large fraction of fine grains compared to Mg AE, Mg–1 cycle, and Mg–3 cycles samples. All Mg2ZnO nanocomposite samples comprised a combination of fine and coarse grains except Mg–2 cycles, which comprised mainly fine grains and a few coarse grains. The little or no change in the grain size of both materials after cyclic CT could be attributed to the change in grain orientation [20], merging of small grains due to compressive stresses leading to formation of coarse grains [5], and the ability of defects to move and accumulate at grain boundaries [22].

Elemental mapping studies revealed O_2 concentration at the porosity as seen in Figure 7a,b. The presence of ZnO nanoparticles was not detected and will require TEM studies.

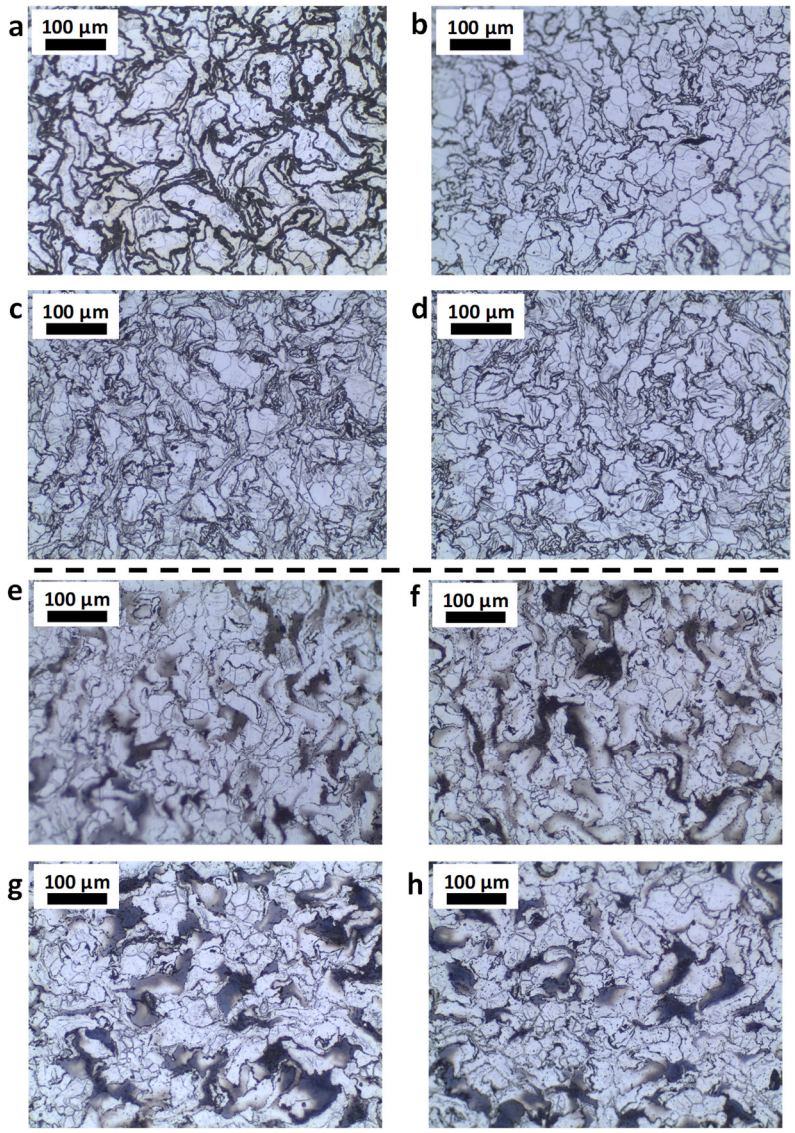

Figure 5. Microstructure of (**a**) Mg AE, (**b**) Mg–1 cycle, (**c**) Mg–2 cycles, (**d**) Mg–3 cycles, (**e**) Mg2ZnO AE, (**f**) Mg2ZnO–1cycle, (**g**) Mg2ZnO–2 cycles, (**h**) Mg2ZnO–3 cycles.

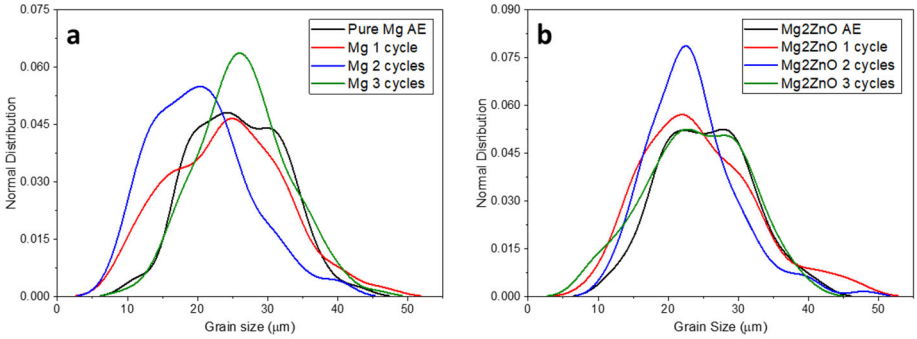

Figure 6. Grain size distribution.

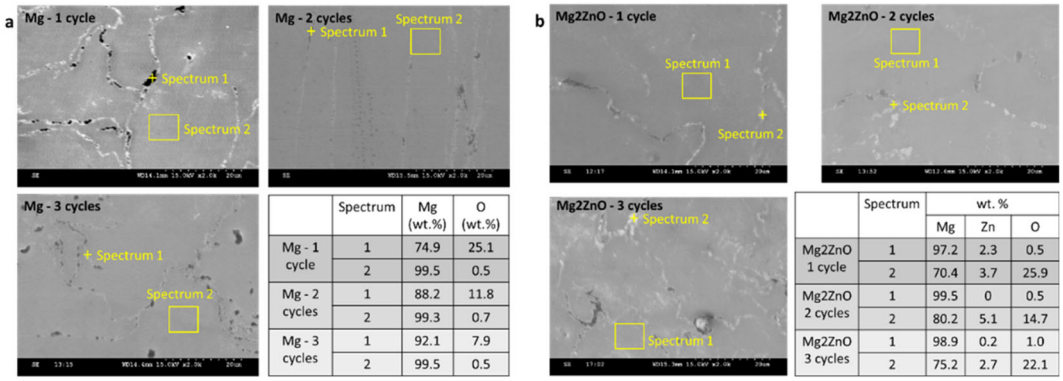

	Spectrum	Mg (wt.%)	O (wt.%)
Mg - 1 cycle	1	74.9	25.1
	2	99.5	0.5
Mg - 2 cycles	1	88.2	11.8
	2	99.3	0.7
Mg - 3 cycles	1	92.1	7.9
	2	99.5	0.5

	Spectrum	wt. %		
		Mg	Zn	O
Mg2ZnO 1 cycle	1	97.2	2.3	0.5
	2	70.4	3.7	25.9
Mg2ZnO 2 cycles	1	99.5	0	0.5
	2	80.2	5.1	14.7
Mg2ZnO 3 cycles	1	98.9	0.2	1.0
	2	75.2	2.7	22.1

Figure 7. Elemental mapping of (**a**) Mg, and (**b**) Mg2ZnO after cyclic CT.

3.3. X-ray Diffraction Analysis

The XRD studies of Mg and Mg2ZnO nanocomposite revealed all Mg peaks except one minor MgO peak as seen in Figure 8a,b. The phases corresponding to different XRD peaks were indexed using JCPDS card number 00-004-0770 for Mg [23] and 00-004-0829 for MgO [23] which was referenced from XRD database [24]. Presence of MgO peak in both materials was attributed to the minor O_2 contamination during processing and it was also confirmed using elemental mapping. The absence of any ZnO peak, as per expected capability of XRD technique, could be attributed to its low amount at 2 wt.% (0.628 vol.%). The pyramidal and basal were the nearly similar dominant textures and basal plane strengthened greatly in pure Mg after cyclic CT as observed from I/I_{max} values from Table 3. However, in Mg2ZnO nanocomposite, pyramidal texture was dominant followed by basal texture and both basal and prism textures strengthened after cyclic CT. Thus the cyclic CT showed ability to strengthen basal texture and randomize crystallographic texture in both Mg and Mg2ZnO nanocomposite materials.

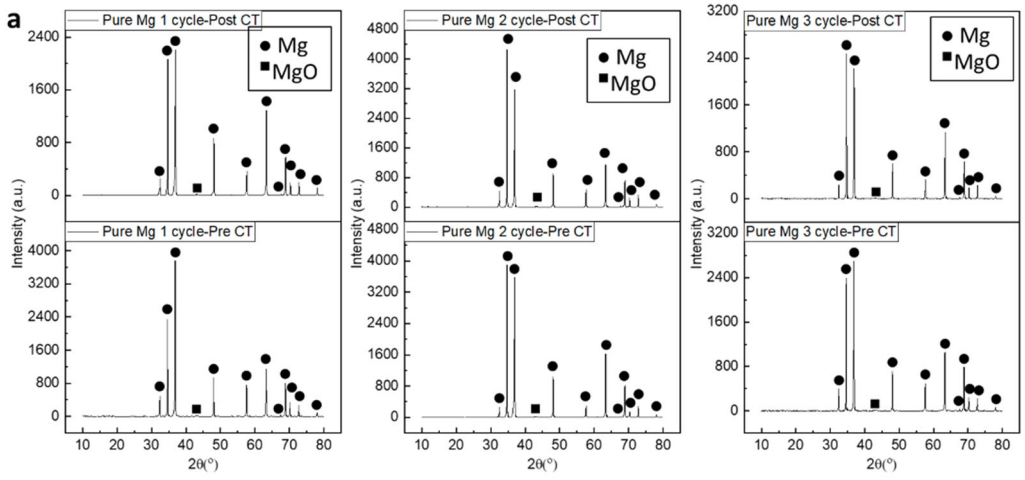

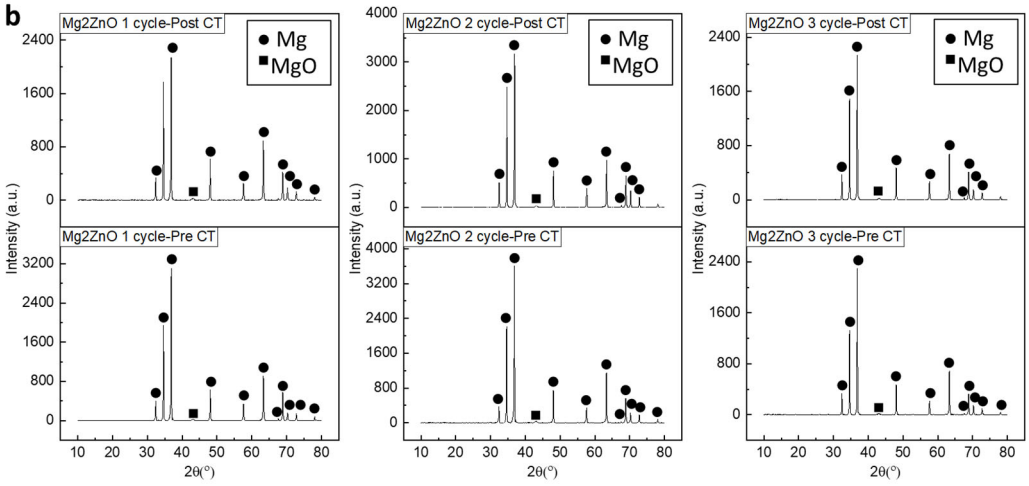

Figure 8. XRD peaks for (**a**) Mg before and after CT; (**b**) Mg2ZnO before and after CT.

Table 3. XRD peak intensity ratios (I/Imax) for different planes.

Material	Plane	Intensity Ratio (I/I_{max})	
		Before CT	After CT
Mg–1 cycle	10-10 Prism	0.130308	0.115890
	0002 Basal	0.619161	0.936623
	10-11 Pyramidal	1	1
Mg–2 cycles	10-10 Prism	0.066359	0.101295
	0002 Basal	1	1
	10-11 Pyramidal	0.91724	0.746886
Mg–3 cycles	10-10 Prism	0.148272	0.098910
	0002 Basal	0.892977	1
	10-11 Pyramidal	1	0.897053
Mg2ZnO–1 cycle	10-10 Prism	0.129063	0.157477
	0002 Basal	0.625040	0.828505
	10-11 Pyramidal	1	1
Mg2ZnO–2 cycles	10-10 Prism	0.103027	0.162930
	0002 Basal	0.613996	0.784654
	10-11 Pyramidal	1	1
Mg2ZnO–3 cycles	10-10 Prism	0.145716	0.175012
	0002 Basal	0.579382	0.696303
	10-11 Pyramidal	1	1

3.4. Damping Analysis

Figure 9a,b show damping response, and Table 4 summarizes the damping characteristics of Mg and Mg/2ZnO nanocomposite before and after cyclic CT. The damping capacity of Mg2ZnO nanocomposite decreased after the addition of ZnO particles. This effect could be understood by Granato–Lücke (G–L) model. According to the G–L model, damping capacity decreases with the increase in the degree of the dislocation pinning. Presence of ZnO particles in the Mg matrix can result in greater dislocation pinning in Mg nanocomposite [25–28]. In addition, the damping capacity of both materials under investigation was reduced after every cycle of the cyclic CT. This could also be attributed to the dislocation pinning due to effects related to CT processing that include a reduction in porosity, an increase in dislocation density, and reduction in grain size. Table 5 depicts the dislocation density values for Mg and Mg2ZnO before and after cyclic CT. the dislocation density is calculated using XRD data. It could be seen that the change in damping capacity is showing similar trend with the dislocation density. The attenuation constant was reduced after cyclic CT for both materials, irrespective of the number of cycles. As per G-L model the lattice deformation leads to generation of thermal energy and/or dislocations in porous materials. This results in internal friction and rapid decay of vibrations giving high attenuation coefficient. Further, the movement of dislocations hinder at the pore boundary and generates high surface energy in this region. Thus, damping capacity is observed to be greater in porous materials [26–28]. Further, the elastic modulus enhanced after the addition of ZnO nanoparticles. This can be attributed to the higher elastic modulus of ZnO nanoparticle

(E = 800 GPa) reinforcement. However, there was no or insignificant change in the elastic modulus of both materials after cyclic CT, except for Mg2ZnO–3 cycles (5.49% increase).

Table 4. Damping and Young's modulus results before and after cyclic CT.

Material	Damping Capacity		Attenuation coefficient		Elastic Modulus (GPa)	
	Before	After	Before	After	Before	After
Mg–1 cycle	0.001631	0.001256 (↓ 22.99%)	59.84	52.08 (↓ 12.97%)	43.56 ± 0.3	43.89 ± 0.4 (↑ 0.75%)
Mg–2 cycle	0.001169	0.000786 (↓ 34.76%)	38.56	33.78 (↓ 12.40%)	45.83 ± 0.4	45.78 ± 0.4 (↓ 0.11%)
Mg–3 cycle	0.000867	0.000862 (↓ 0.58%)	31.49	30.03 (↓ 4.64%)	44.11 ± 0.4	44.08 ± 0.4 (↓ 0.07%)
Mg2ZnO–1 cycle	0.000490	0.000478 (↓ 2.45%)	21.19	19.41 (↓ 8.40%)	46.66 ± 0.3	46.79 ± 0.4 (↑ 0.28%)
Mg2ZnO–2 cycles	0.000475	0.000396 (↓ 16.31%)	19.58	15.85 (↓ 19.05%)	47.62 ± 0.3	47.73 ± 0.4 (↑ 0.23%)
Mg2ZnO–3 cycles	0.000413	0.000410 (↓ 0.72%)	16.50	19.49 (↓ 18.12%)	47.71 ± 0.4	50.33 ± 0.4 (↑ 5.49%)

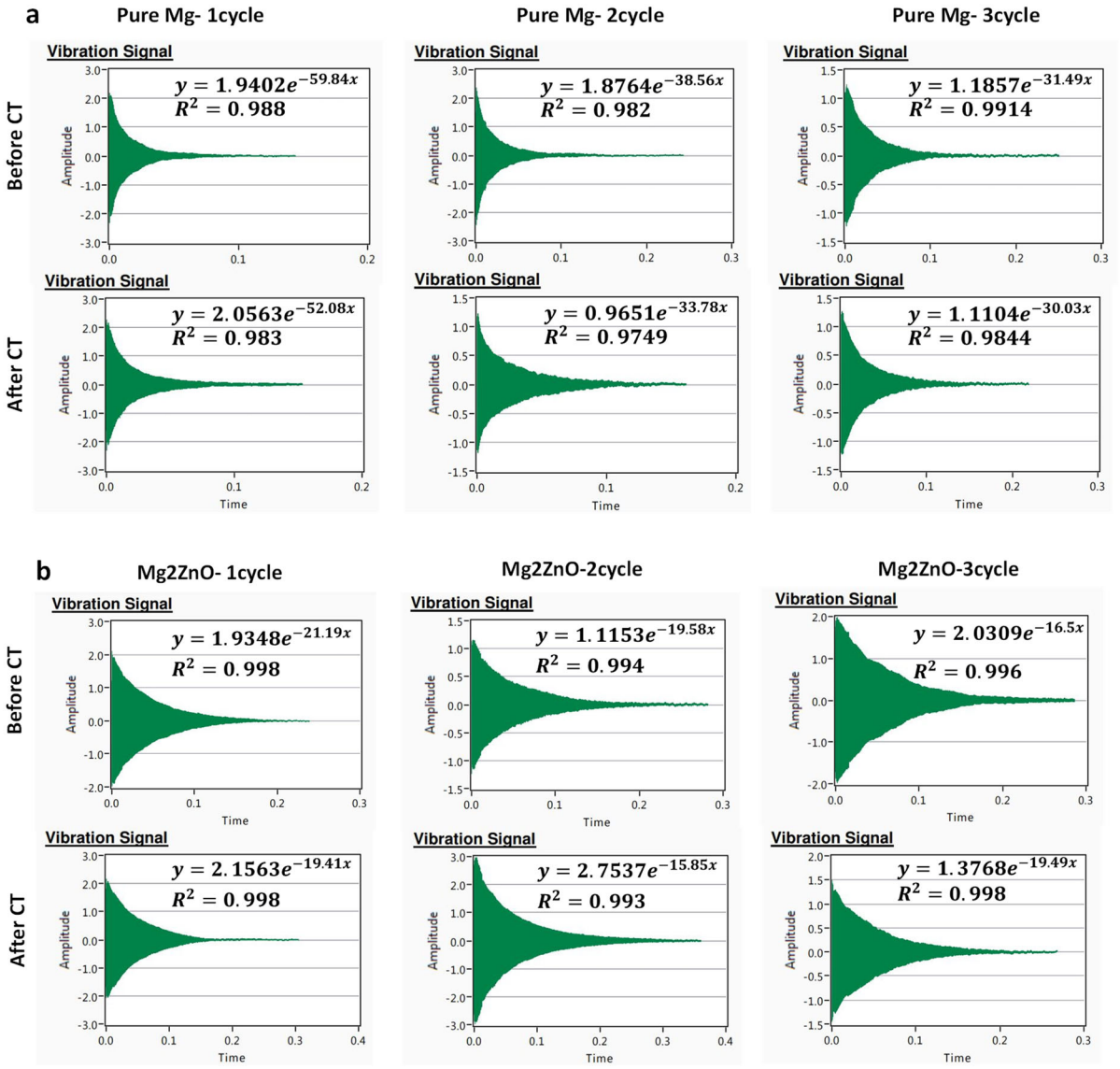

Figure 9. Damping plots and attenuation coefficient in AE and cyclic CT condition for (a) Mg; and (b) Mg2ZnO.

Table 5. Dislocation density before and after cyclic CT.

Material	Dislocation Density $\times$ 10^{-3} (nm^{-2})	
	Before	**After**
Mg–1 cycle	0.333	0.362
Mg–2 cycles	0.246	0.239
Mg–3 cycles	0.297	0.305
Mg2ZnO–1 cycle	0.377	0.453
Mg2ZnO–2 cycles	0.408	0.532
Mg2ZnO–3 cycles	0.412	0.471

3.5. Hardness Measurement

Figure 10 shows the hardness of Mg and Mg2ZnO nanocomposite before and after cyclic CT. Hardness increased after the addition of nanoparticles due to high hardness [29] and near uniform distribution of ZnO nanoparticles (Figure 2). However, Mg showed a slight decrease in the hardness after every cycle of CT. On the contrary, the Mg2ZnO composites exhibited slightly greater hardness after 1 cycle and 2 cycles and a slight decrease in hardness after 3 cycles of CT. It was observed that the hardness variations were not significant, and values fell inside the standard deviation. Thus, the slight changes in hardness could be attributed to the combined effect of the change in density, grain size distribution, and dislocations.

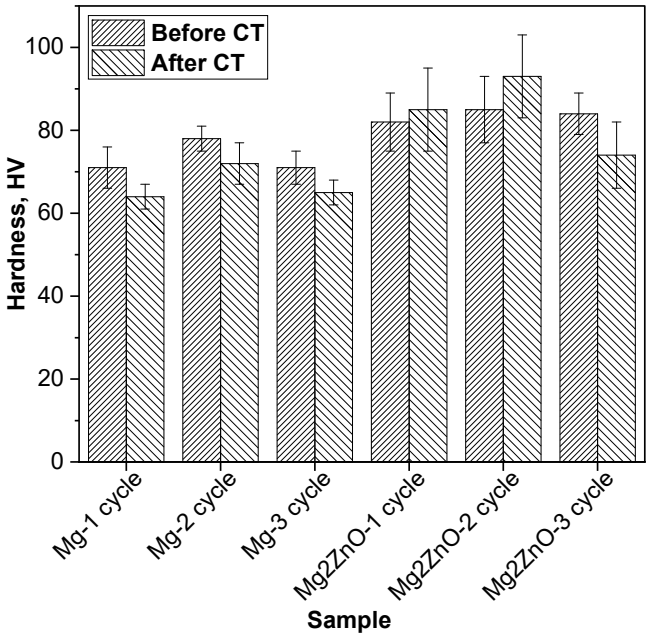

Figure 10. Microhardness before and after cyclic CT.

3.6. Compression Behavior

Figure 11 shows representative compressive stress-strain curves for both materials in as-extruded and after different cyclic CT. It was seen that 0.2 CYS, UCS, fracture strain, and energy absorbed increased by 13.88%, 25.88%, 15.28%, and 63.64%, respectively, after addition of ZnO nanoparticles in Mg. This could be attributed to the particle reinforcement strengthening due to the ZnO. Compressive strengths of Mg decreased slightly after cyclic CT while fracture strain and energy absorbed showed slight increases. As seen in Table 6, the change in compressive properties of Mg for different cycles of CT were almost similar with values falling inside standard deviation range. On the contrary to Mg, compressive strengths of Mg_2ZnO nanocomposite increased after cyclic CT. Fracture strain remained constant for Mg_2ZnO–1 cycle and Mg_2ZnO–2 cycles, while reduced slightly for Mg_2ZnO–3 cycles. Energy absorbed increased for Mg2ZnO–1 cycle and Mg_2ZnO–2 cycles, while reduced considerably for Mg_2ZnO–3 cycles. Thus, Mg_2ZnO–2 cycles sample exhibited superior combination of compressive strength, fracture strain, and energy absorbed. The enhanced strength after cyclic CT could be attributed to the textural changes, better matrix-reinforcement interfacial bonding owing to the contraction of Mg matrix against the ZnO particulates, and greater compressive stresses arising from the presence of two phases (Mg and ZnO). The formation mechanism of enhanced matrix-interfacial bonding and increased compressive stresses

has been explained in detail by Gupta et al. [13] and Mirza et al. [30]. Moreover, the Orowan strengthening and Zener pinning effect could be possible additional strengthening mechanisms.

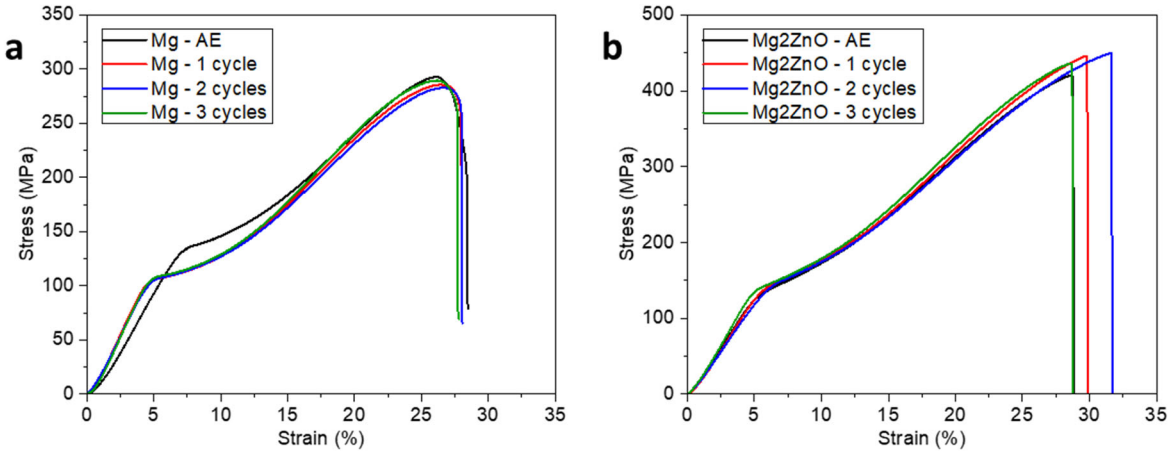

Figure 11. Representative compression stress vs strain curves at different conditions for (**a**) Mg, and (**b**) Mg2ZnO nanocomposite.

Tun et al. [3] fabricated Mg–ZnO nanocomposites using a microwave sintering technique followed by extrusion. Although 0.2 CYS of Mg increased from ~103 to ~109 MPa, fracture strain decreased from ~22% to 14% with the addition of nano-ZnO particles, UCS increased from 263 to 368 MPa with increase in ZnO nanoparticles content. A study by Sankarayanan et al. [16] Mg-ZnO nanocomposites synthesized using disintegration melt deposition revealed that 0.2% compressive yield strength of Mg increased by ~50%, ~67%, and ~90% with the vol.% of ZnO addition of 0.16, 0.48, and 0.8, respectively. Besides, fracture strain of ~ 22% remained constant with and without the addition of ZnO nanoparticles. The study reported better combination of properties with 0.2 CYS of ~345 MPa and a fracture strain of ~22%. In the present study, with the addition of 2 wt.% ZnO nanoparticles, the enhancement in 0.2 CYS and fracture strain is achieved by 13.88% and 63.64%, respectively. Thus, a superior combination of properties with 0.2 CYS and a fracture strain of 123 MPa and 72%, respectively, is obtained in this work.

Table 6. Compressive properties Mg and Mg2ZnO nanocomposite before and after cyclic CT.

Material	0.2 CYS (MPa)	UCS (MPa)	Fracture Strain (%)	Energy Absorbed (MJ/m^2)
Mg AE	108 ± 13	170 ± 9	26 ± 2	44 ± 5.6
Mg–1 cycle	101 ± 1 (↓ 6.5%)	157 ± 7 (↓ 7.6%)	27 ± 0.9 (↑ 3.8%)	45 ± 2.6 (↑ 2.2%)
Mg–2 cycles	96 ± 1 (↓ 11.1%)	162 ± 3 (↓ 4.7%)	27 ± 0.7 (↑ 3.8%)	45 ± 1.5 (↑ 2.2%)
Mg–3 cycles	99 ± 5 (↓ 8.33%)	161 ± 5 (↓ 5.94%)	27 ± 1.0 (↑ 3.8%)	44 ± 2.9
Mg_2ZnO AE	123 ± 4	214 ± 5	30 ± 1.5	72 ± 4.7
Mg2ZnO–1 cycle	135 ± 4 (↑ 9.76%)	222 ± 3 (↑ 3.74%)	30 ± 0.5	74 ± 3.4 (↑ 2.70%)
Mg2ZnO–2 cycles	136 ± 3 (↑ 10.57%)	224 ± 8 (↑ 4.67%)	30 ± 1.1	78 ± 3.2 (↑ 8.33%)
Mg2ZnO–3 cycles	134 ± 3 (↑ 8.94%)	222 ± 3 (↑ 3.74%)	29 ± 0.7 (↓ 3.33%)	66 ± 0.8 (↓ 8.33%)

3.7. Fracture Behaviour

Figure 12 shows SEM micrographs of compressive fractured surfaces of cyclic CTed Mg and Mg2ZnO nanocomposite Fractography revealed the presence of shear bands (hollow arrows) and rough surface. Cryogenic treatment did not result in qualitative differences on the fracture surface morphology. Under compressive loading conditions, concentrated shear stresses can initiate shear band formation which are narrow zones of localized deformation [31]. Thus, appearance of rough surfaces indicating plastic deformation, cleavage surfaces, and shear

bands was expected. To note that fracture strain of both monolithic and composite samples remained in 26–30% range which is very reasonable. Under compressive loading, after a certain amount of plastic deformation, the material ruptures rapidly, exhibiting both ductile and brittle fracture modes [32].

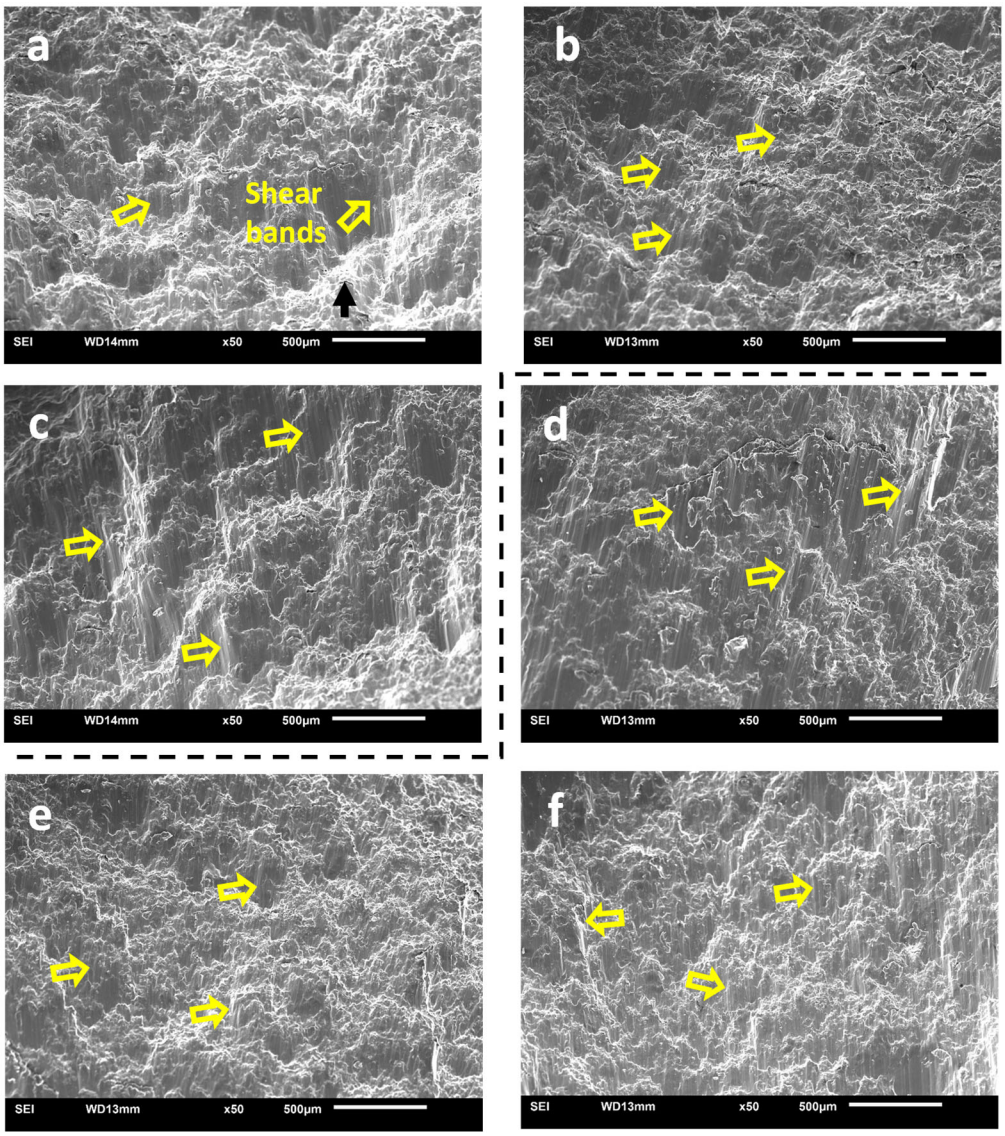

Figure 12. SEM fractographs for compressive fractured surfaces of samples (**a**) Mg–1 cycle, (**b**) Mg–2 cycles, (**c**) Mg–3 cycles, (**d**) Mg2ZnO–1 cycle, (**e**) Mg2ZnO–2 cycles, (**f**) Mg2ZnO–3 cycles.

4. Conclusions

Pure Mg and Mg2ZnO nanocomposites were successfully synthesized and subjected to cyclic cryogenic treatment. A comparative study on the properties of both materials was performed in detail, and key conclusions are summarized below:

(a) The addition of 2 wt.% ZnO nanoparticles in pure Mg did not affect the amount of porosity and grain size of pure magnesium.
(b) The porosity reduction was maximum for 3 cycles of cryogenic treatment for pure Mg (69%) and 2 cycles of CT for Mg2ZnO nanocomposite (68%)
(c) The average grain size reduction was best for 2 cycles of CT for both pure Mg and Mg2ZnO.
(d) Textural changes were observed in both materials after all cyclic CT.
(e) Though there was a reduction in damping capacity of both materials irrespective of cyclic CT, the maximum reduction of ~35% and ~16%, respectively was observed for Mg and Mg2ZnO after 2 cycles of CT. The elastic modulus remained nearly constant for both materials even after cyclic CT except the noticeably increase of 5.5% was observed for Mg2ZnO–3 cycles.

(f) The addition of ZnO particles increased the hardness of pure Mg. Cryogenic heat treatment led only to a reduction in the hardness of pure Mg. In the case of Mg2ZnO, the best improvement was realized after 2 cycles of CT (9.4%).
(g) The compressive mechanical properties such as 0.2 compressive yield strength, ultimate compressive strength, fracture strain, and elastic modulus increased by 13.88%, 25.88%, 15.28%, and 9.53% after the addition of ZnO nanoparticles.
(h) The maximum of 2.2% and 8.33% increase in energy absorbed in Mg and Mg2ZnO was obtained after 2 cycles of CT. In all cases, energy absorbed, which reflects the synergy between strengths (CYS and UCS) and failure strain, increased following cryogenic treatments except for Mg2ZnO with 3 cycles of CT.
(i) Cyclic cryogenic treatment reduced 0.2CYS and UCS of pure magnesium while increasing average failure strain from 26% to 27%. For Mg2ZnO, 0.2CYS and UCS increased for all cycles of cryogenic treatments. Failure strain remained constant for 1 and 2 cycles of CT and reduced from an average value of 30% to 29% for 3 cycles of cryogenic treatment.

The present study suggests that cyclic cryogenic treatment has the capability of positively changing the strength properties of nanocomposites. For Mg2ZnO, it is 2 cycles of cryogenic treatment which gives the best combination of properties. For pure magnesium, the overall effect of cryogenic treatment is almost negligible.

Author Contributions: P.D.: Data curation, Formal analysis, Investigation, Visualization, Writing—original draft, Writing—review & editing; M.J.: Data curation, Resources, Formal analysis, Investigation, Supervision, Validation, Visualization, Methodology, Writing—review & editing; D.S.: Supervision, Project administration; M.G.: Conceptualization, Resources, Supervision, Validation, Methodology, Project administration, writing—review & editing. All authors have read and agreed to the published version of the manuscript.

Funding: This research received no funding.

Data Availability Statement: The original contributions presented in the study are included in the article, further inquiries can be directed to the corresponding author.

Acknowledgments: The authors would like to thank Juraimi Bin Madon for his assistance in extruding the materials studied in this work.

Conflicts of Interest: The authors declare no conflict of interest.

References

1. Wong, W.L.E.; Gupta, M. Development of Mg/Cu Nanocomposites Using Microwave Assisted owder Metallurgy Technique. In Proceedings of the ASME 2005 International Mechanical Engineering Congress and Exposition, Orlando, FL, USA, 5–11 November 2005.
2. Gupta, M.; Wong, W.L.E. Magnesium-Based Nanocomposites: Lightweight Materials of the Future. *Mater. Charact.* **2015**, *105*, 30–46.
3. Tun, K.S.; Jayaramanavar, P.; Nguyen, Q.B.; Chan, J.; Kwok, R.; Gupta, M. Investigation into Tensile and Compressive Responses of Mg-ZnO Composites. *Mater. Sci. Technol.* **2012**, *28*, 582–588. https://doi.org/10.1179/1743284711Y.0000000108.
4. Ahmad, I.R.; Jing, X.; Shu, D.W. Effect of Temperature on the Mechanical Behaviour of Magnesium Alloy AZ91D in the Range between −30 °C and 250 °C. *Int. J. Mech. Sci.* **2014**, *86*, 34–45. https://doi.org/10.1016/j.ijmecsci.2014.04.010.
5. Gupta, S.; Parande, G.; Gupta, M. Comparison of Shallow (−20 °C) and Deep Cryogenic Treatment (−196 °C) to Enhance the Properties of a Mg/2wt.% CeO2 Nanocomposite. *Technologies* **2024**, *12*, 14. https://doi.org/10.3390/technologies12020014.
6. Hassan, S.F.; Ho, K.F.; Gupta, M. Increasing Elastic Modulus, Strength and CTE of AZ91 by Reinforcing Pure Magnesium with Elemental Copper. *Mater. Lett.* **2004**, *58*, 2143–2146. https://doi.org/10.1016/j.matlet.2004.01.011.
7. Hassan, S.F.; Gupta, M. Development of Ductile Magnesium Composite Materials Using Titanium as Reinforcement. *J. Alloys Compd.* **2002**, *345*, 246–251.
8. Kainer, K.U. *Magnesium Alloys and Technologies*; Wiley-VCH: Hoboken, NJ, USA, 2003; ISBN 352730570X.
9. Eugene, W.W.L.; Gupta, M. Enhancing Thermal Stability, Modulus and Ductility of Magnesium Using Molybdenum as Reinforcement. *Adv. Eng. Mater.* **2005**, *7*, 250–256. https://doi.org/10.1002/adem.200400137.
10. Lloyd, D.J. Particle Reinforced Aluminium and Magnesium Matrix Composites; *Int. Mater. Rev.* **1994**, *39*, 1–23.

11. Nie, K.B.; Wang, X.J.; Deng, K.K.; Hu, X.S.; Wu, K. Magnesium Matrix Composite Reinforced by Nanoparticles—A Review. *J. Magnes. Alloys* **2021**, *9*, 57–77.
12. Wong, W.L.E.; Gupta, M. Development of High Performance Mg/SiC Composites Containing Nano-Size SiC Using Microwave Assisted Rapid Sintering. *Am. Soc. Mech. Eng. Aerosp. Div.* **2005**, *70*, 511–515. https://doi.org/10.1115/IMECE2005-82501.
13. Gupta, S.; Parande, G.; Tun, K.S.; Gupta, M. Enhancing the Physical, Thermal, and Mechanical Responses of a Mg/2wt.%CeO2 Nanocomposite Using Deep Cryogenic Treatment. *Metals* **2023**, *13*, 660. https://doi.org/10.3390/met13040660.
14. Parande, G.; Manakari, V.; Meenashisundaram, G.K.; Gupta, M. Enhancing the Hardness/Compression/Damping Response of Magnesium by Reinforcing with Biocompatible Silica Nanoparticulates; *Int. J. Mater. Res.* **2016**, *107*, 1–9. https://doi.org/10.3139/146.111435.
15. Tun, K.S.; Gupta, M. Improving Mechanical Properties of Magnesium Using Nano-Yttria Reinforcement and Microwave Assisted Powder Metallurgy Method. *Compos. Sci. Technol.* **2007**, *67*, 2657–2664. https://doi.org/10.1016/j.compscitech.2007.03.006.
16. Sankaranarayanan, S.; Pranav Nayak, U.; Sabat, R.K.; Suwas, S.; Almajid, A.; Gupta, M. Nano-ZnO Particle Addition to Monolithic Magnesium for Enhanced Tensile and Compressive Response. *J. Alloys Compd.* **2014**, *615*, 211–219. https://doi.org/10.1016/j.jallcom.2014.06.163.
17. Kalsi, N.S.; Sehgal, R.; Sharma, V.S. Cryogenic Treatment of Tool Materials: A Review. *Mater. Manuf. Process.* **2010**, *25*, 1077–1100.
18. Kalia, S. Cryogenic Processing: A Study of Materials at Low Temperatures. *J. Low. Temp. Phys.* **2010**, *158*, 934–945. https://doi.org/10.1007/s10909-009-0058-x.
19. Dong, N.; Sun, L.; Ma, H.; Jin, P. Effects of Cryogenic Treatment on Microstructures and Mechanical Properties of Mg-2Nd-4Zn Alloy. *Mater. Lett.* **2021**, *305*, 130699. https://doi.org/10.1016/j.matlet.2021.130699.
20. Jiang, Y.; Chen, D.; Chen, Z.; Liu, J. Effect of Cryogenic Treatment on the Microstructure and Mechanical Properties of AZ31 Magnesium Alloy. *Mater. Manuf. Process.* **2010**, *25*, 837–841. https://doi.org/10.1080/10426910903496862.
21. Huang, H.; Zhang, J. Microstructure and Mechanical Properties of AZ31 Magnesium Alloy Processed by Multi-Directional Forging at Different Temperatures. *Mater. Sci. Eng. A* **2016**, *674*, 52–58. https://doi.org/10.1016/j.msea.2016.07.052.
22. Sonar, T.; Lomte, S.; Gogte, C. Cryogenic Treatment of Metal-A Review; *Mater. Today: Proc.* **2018**, *5*, 5219–25228.
23. Pahaul, A.; Johanes, M.; Gupta, M. A First-Time Addition of Selenium to a Mg-Based Metal Matrix Composite for Biomedical Purposes. *J. Compos. Sci.* **2024**, *8*, 81. https://doi.org/10.3390/jcs8030081.
24. Gates-Rector, S.; Blanton, T. The Powder Diffraction File: A Quality Materials Characterization Database. *Powder Diffr.* **2019**, *34*, 352–360. https://doi.org/10.1017/S0885715619000812.
25. Wan, D.; Hu, Y.; Ye, S.; Li, Z.; Li, L.; Huang, Y. Effect of Alloying Elements on Magnesium Alloy Damping Capacities at Room Temperature. *Int. J. Miner. Metall. Mater.* **2019**, *26*, 760–765. https://doi.org/10.1007/s12613-019-1789-6.
26. Zhang, J.; Gungor, M.N.; Lavernia, E.J. The Effect of Porosity on the Microstructural Damping Response of 6061 Aluminium Alloy. *J. Materials Science***, 1993**, *28*, 1515–1524.
27. Li, Q.; Jiang, G.; Dong, J.; Hou, J.; He, G. Damping Behavior and Energy Absorption Capability of Porous Magnesium. *J. Alloys Compd.* **2016**, *680*, 522–530.
28. Granato, A.; Lücke, K. Theory of Mechanical Damping Due to Dislocations. *J. Appl. Phys.* **1956**, *27*, 583–593. https://doi.org/10.1063/1.1722436.
29. Advertise with MatWeb! Zinc Oxide, ZnO, (Zincite) Categories: Ceramic; Oxide; 1996. Available online: https://www.vedantu.com/chemistry/zinc-oxide (accessed on 2 July 2024).
30. Mirza, F.A.; Chen, D.L. A Unified Model for the Prediction of Yield Strength in Particulate-Reinforced Metal Matrix Nanocomposites. *Materials* **2015**, *8*, 5138–5153. https://doi.org/10.3390/ma8085138.
31. Radford, D.D.; Willmott, G.R.; Walley, S.M. Failure Mechanism in Ductile and Brittle Materials During Taylor Impact. *J. Phys. IV Fr.* **2003**, *110*, 687.
32. Chen, Y.; Cao, F.; Deng, C.; Zhang, Y. Effect of compression loading speeds on the room temperature mechanical properties of as-extruded AZ31 magnesium alloy. *Phys. Conf. Ser.* **2022**, *2174*, 012065. https://doi.org/10.1088/1742-6596/2174/1/012065.